Effective gray-scale in lithographically-scribed planar holographic Bragg reflectors

D. Iazikov*, C. Greiner and T. W. Mossberg
LightSmyth Technologies, Inc., 860 W. Park St., Ste 250, Eugene, OR 97041

ABSTRACT

We demonstrate that holographic Bragg reflector grating structures, photolithographically scribed in planar waveguides, support a unique approach to apodization and overlay that uses fixed-depth etching and partial contour writing to achieve continuous reflective amplitude control.

Keywords: Integrated Optics, Bragg Reflector, Planar Waveguide, Lithography, Holography

1. INTRODUCTION

Distributed Bragg reflectors (DBR's) can in principle be structured so as to provide a wide range of spectral filtering functions. In the limit of weak reflectivity, the reflection spectrum of a DBR is simply related to the spatial Fourier transform of its effective reflection coefficient expressed as a function of optical depth into the reflector. Continuous control over the DBR's reflective strength and relative phase as a function of position thus provides the ability to implement arbitrary phase-coherent spectral filtering functions. In the limit of strong reflectivity, the relationship of local reflective amplitude and phase to the spectral transfer function is more complex, but the ability to implement broad ranges of filtering functions remains. Key to the realization of specific filtering functions is the ability to precisely control reflective amplitude and phase as a function of depth within the DBR – even down to the level of individual diffractive elements (lines or planes within the diffractive structure).

Tailoring of DBR spectral filtering functions has been demonstrated in the case of fiber Bragg gratings[1-7] and channel-waveguides[8-10] by a variety of techniques. Yet none of those provides for very high resolution (approaching line-by-line) control of diffractive element amplitude and phase. Recently, a new type of slab waveguide DBR has been proposed[11] and demonstrated[12]. These wholly in-plane diffractive structures are referred to as holographic Bragg reflectors (or HBRs) and comprise computer-generated holograms lithographically scribed into the core of a 2D slab waveguide. HBRs are compatible with truly line-by-line amplitude and phase apodization by means that we explore here. The diffractive elements of an HBR typically consist of lithographically scribed contours filled with cladding or other dielectric material having a refractive index differing from that of the core. HBRs control both the spatial wavefront of reflected signals and their spectral content. In principle, HBRs provide a path to unique optical circuits based not on constraining wire-like channel waveguides but integrated, overlapping HBRs that spectrally process and spatially route freely intersecting optical data streams from one active circuit element to another. HBRs provide the power of free-space optics in a fully integrated environment. HBR structures, whose computer-generated diffractive contours provide broad in-plane spatial wavefront transformation capability, contrast with previously discussed lithographically scribed 2D DBRs intended for out-of-plane applications such as laser feedback and outcoupling[13-18] and free-space to slab-waveguide beam coupling[19-21]. Also, the use of holographic imaging possible with HBRs is generally more powerful than that provided by confocal elliptical DBRs that have been discussed in terms of spectral multiplexing[22].

* e-mail: diazikov@lightsmyth.com, phone: (541) 431-0026, fax: (541) 284-5607

2. RESULTS AND DISCUSSION

A simple HBR is schematically shown in Figure 1. Light enters the slab waveguide region at the IN port and expands within the plane to interact with the multitude of diffractive elements (curved contours). Each diffractive element serves as an imaging device focusing the input signal to the OUT port. For an HBR operating in m^{th} order, diffractive elements are spaced approximately by a distance $\Lambda = m \times \lambda / 2n_{eff}$ ($m=1,2,3\ldots$), where λ is the vacuum wavelength of the light to be reflected and n_{eff} is the effective refractive index of the slab waveguide. In Figure 1 and in the fabricated devices discussed here, the diffractive elements comprise circular cladding-filled trenches scribed in the top of the slab waveguide core layer via DUV photolithography. All diffractive elements share a common center of curvature. As measured along a radius through the center of curvature, the diffractive elements do not have a constant spacing. The spacing is set so that signals propagating between the input and output ports via interaction with the diffractive elements see a constant optical path increment of $m \times \lambda / 2n_{eff}$ between diffractive elements.[11] This results in a weak chirp in diffractive element spacing as measured along a line through the center of curvature. We refer to the line containing the access ports as input or output plane as appropriate.

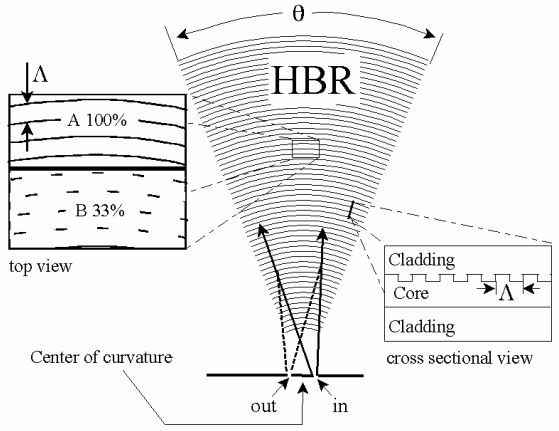

Figure 1. Schematic of a holographic Bragg reflector (HBR). Curved contours represent diffractive elements lithographically scribed in a slab waveguide. Each contour backscatters a portion of the entering signal field and focuses it onto the output port. In the devices fabricated for this study, the contours are circular with common center of curvature shown. In the blow-up to the left, the partial-fill effective gray scale approach to amplitude apodization is shown. The fraction of the contour actually populated with an etched trench controls the overall effective amplitude of the field backscattered to the output port by the contour.

Optimal flexibility in designing of spectral transfer functions requires control over the reflective amplitude and relative phase of each diffractive element. Relative reflective phase shifts over the range of $\pm\pi$ are provided by spatially displacing diffractive contours over a range $\pm\lambda / 4n_{eff}$. Since HBR contours comprise a computer-generated hologram, which is laser or e-beam written onto a standard reticle, and photolithographically scribed onto slab waveguides, full positioning (and hence phase control over reflective phase) is conveniently available. The reflective amplitude of a trench-like reflective element is determined by various factors such as trench depth, trench width, refractive index contrast between the core and fill materials, etc. While these factors can in principle be used to control the reflective amplitude of the diffractive elements, their practical implementation is inconsistent with convenient lithographic practice which typically employs a common etch depth across each wafer, uses a single trench-fill material, and is subject to process-related trench width variations.

However, as we demonstrate here, the 2D nature of HBR devices allows them to be implemented with diffractive elements of variable reflective amplitude using only straightforward lithographic techniques. Referring to Figure 1 and considering monochromatic input light, one can see that a single diffractive element contour, k , contributes, an amount to the output signal field given by

$$E_{out}^{k} \propto \int_{contour\ k} E_{in}(\vec{r}) a_k(\vec{r}) \qquad (1)$$

where $E_{in}(\vec{r})$ and $a_k(\vec{r})$ are, respectively, the input field and amplitude reflection coefficient at contour position $\vec{r}$. It is assumed that the HBR has been designed so that contributions to the output field from all locations on the single contour arrive with the same phase – a necessary condition for effective imaging. Eq. 1 implies that partial contour scribing (i. e. creating a trench along only selected portions of a diffractive element contour) provides a means of continuously controlling the contour's contribution to the output field without the need for lithographically challenging variations in diffractive-element trench morphology.

While the partial scribing approach to achieving continuous reflective amplitude control for individual diffractive elements is conceptually simple, many details must be considered. In order to preserve the focusing character of the HBR, the partially written diffractive contours must generate substantially the same output wavefront as the fully written diffractive-element contour. The variation in input field amplitude along the contour must be either explicitly considered in determining which portions of a contour to fill, or a fill pattern must be adopted that is immune to a range of input field variations. Furthermore, correlation in fill pattern between successive diffractive elements must be considered to ensure that portions of the input field do not "leak" through holes in the HBR structure. Finally, since the effective waveguide refractive index is perturbed, albeit weakly, by the presence of diffractive element trenches, spatial variations in the effective index introduced by partial scribing must be explicitly accounted for in the HBR design process. We refer to the partial writing of diffractive element contours in HBR devices as "effective gray scale."

We have fabricated HBR structures to test certain aspects of the effective gray scale concept. We wish to compare HBRs written with a fixed 0.33 fraction of each contour scribed to HBRs having fully written contours in regards to 1) overall spectral transfer function, 2) relative reflective strength and 3) spatial focusing properties. First- and third-order HBRs were fabricated with completely filled (i. e. scribed) diffractive element contours. A second first-order HBR was partially scribed, i. e. only 1/3 of each diffractive contour was etched to produce a trench. Blow-ups of the diffractive contours of these HBRs are shown in Figure 2. Figure 2c shows how, in the case of the partially written HBR each contour was divided into 20 equal angular segments of angular width θ_k, and 1/3 of each angular segment was lithographically

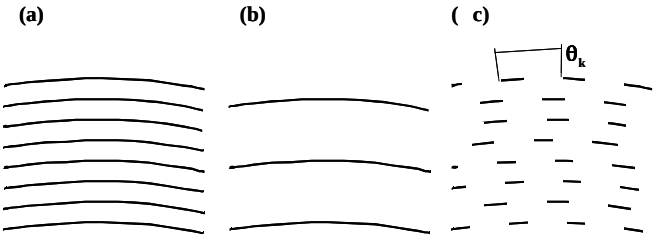

Figure 2. Blow-up view of the diffractive contours of the fully-scribed first-order (a), third-order (b) and partially-scribed (0.33 grey scale, c) HBR. θ_k, angular subsegment.

scribed to produce a trench. As previously mentioned, unlike in the simple HBR schematic of Figure 1b, diffractive contours of the actual HBRs subtend increasingly smaller angles as one moves away from the input/output plane. Owing to this variation in total angular width subtended by the diffractive contours, θ_k ranges from 0.0165 to 0.0265 rad. The angular segments of successive diffractive elements were given random angle shifts of magnitude $\eta_k\theta_k$, where η_k is randomly generated from the interval (0,1) for each contour.

We first consider the overall spectral transfer function and reflective strength of HBRs implemented with effective gray scale (partial contour scribing). To this end, in Figure 3, we compare spectra and reflected power levels of a first-order, partially written, 0.33-fill-factor HBR (dotted line) and a third-order fully written, 1.0-fill-factor HBR (solid line). The partially written HBR has 33 percent of each contour written as described above. For the spectral measurement, a die equipped with input and output channel waveguides was employed. Actual spectra are obtained by scanning a fixed-polarization test laser across the HBR reflective peak. In Figure 3, all data is multiplied by the same constant factor so that the peak of the solid curve equates to unity. Differences between the solid and dotted line are preserved. It is seen that the first-order, 0.33-written HBR and the third-order, 1.0-written HBR have essentially identical reflectivity. This result is fully consistent with our premise that fill-factor equates to diffractive amplitude. Applying the gray-scale concept to Figure 3, we expect that reflected power should scale as the total number of diffractive contours in the HBR multiplied by the fill-factor (reflective amplitude) of the contours. Thus we expect the first-order, 0.33-written HBR and third-order, 1.0-written HBR to have the same reflectivity – as indeed they do.

From Figure 3, we also see that the reflection spectra of the partially written and completely written HBRs are virtually identical as one would expect for first and third order HBRs of the same length whose only difference is the reflective amplitude of diffractive elements. To facilitate comparison of the spectra, they have been horizontally shifted to a common wavelength origin. The actual peak reflection wavelengths of the two HBRs are 1530.93 nm and 1530.75 nm for the first-order, 0.33-filled and third-order, 1.0-filled HBR, respectively.

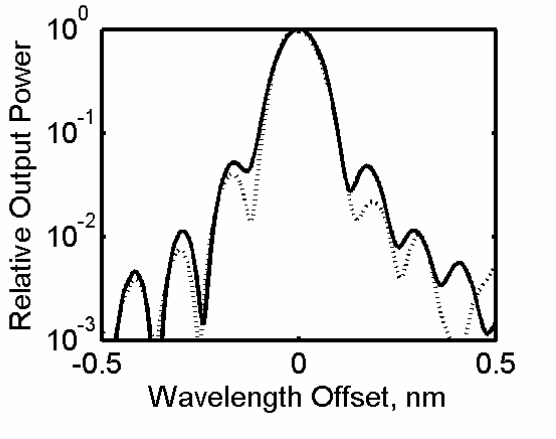

Figure 3. Superimposed reflection spectra of a 0.33 gray-scale first-order HBR (dotted line) and a fully written third-order HBR. Spectral widths and peak reflectivity are essentially identical confirming the ability of partial-fill gray scale to control reflection amplitude.

Next, we consider the imaging properties of HBRs implemented with effective gray scale (partial contour scribing). The division of each diffractive element contour into 20 partially scribed segments provides for high fidelity sampling of the input signal beam. On the other hand, introduction of a non-continuous, grating-like structure to the diffractive contour can in certain cases introduce ghost structures in the output plane. Theoretical simulation and HBR measurement reveal that ghosts structures are greatly suppressed in HBR structures with large numbers of diffractive elements by two implemented design factors, i. e. the random angular shifts described above and by the variation in angular segment size.

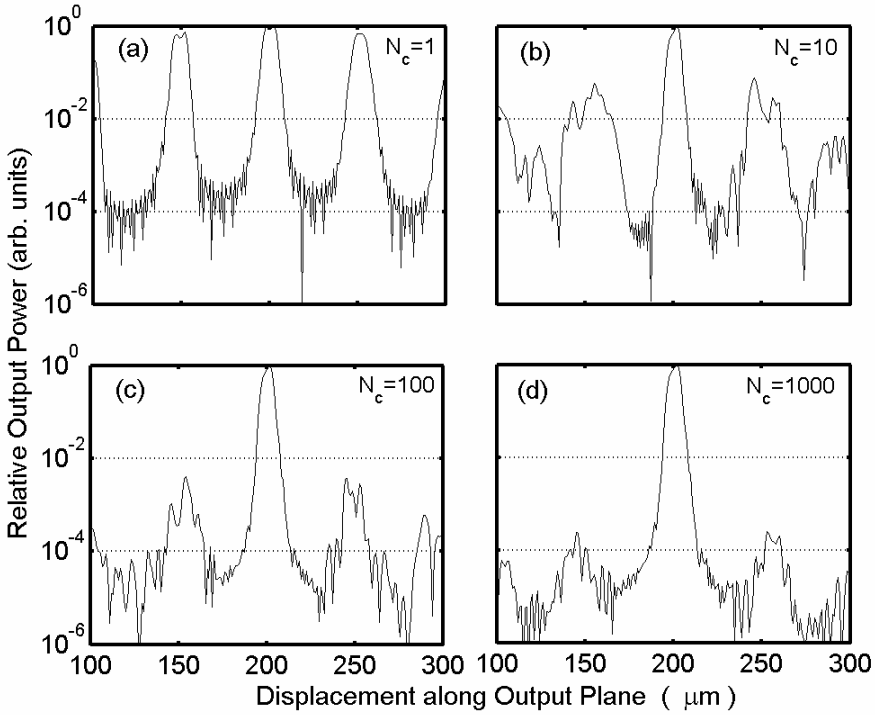

Figure 4. Simulated output power as a function of position along output plane for (a)-(d) 1, 10, 100, and 1000 partially written diffractive contours showing the decrease in sidelobe power with increasing contour count. The primary output image is located at 200 μm.

In Figure 4, we show calculated power as a function of position along the output plane of an HBR with partially scribed diffractive contours and various numbers, N_c, of diffractive contours. Except for Figure 4a which depicts the power distribution produced by a single diffractive contour (N_c = 1) positioned in the middle of the fabricated structure, contours are distributed uniformly throughout the same physical region as the fabricated HBRs. Contour spacing and hence effective diffractive order are adjusted as necessary. Calculations of the output power profile are obtained by representing the HBR structures as point scatterers densely spaced along the etched diffractive trenches. Output plane powers shown are derived from an explicit summation of fields diffracted from the input port (10-μm-wide with a rectangular field profile), scattered by the representative structure points, and received along the output plane. The input port is positioned at -200 μm, the diffractive-element center of curvature at 0, which places the nominal output port location at +200 μm.

In Figure 4a, the power distribution created by a single partially written contour shows a primary image at +200 μm as well as sidelobes of nearly equal strength. The sidelobes correspond to diffractive orders of the segmented contour viewed as a reflective diffraction grating. The side lobes appear equally spaced about the primary image by a distance $\lambda/\sin\theta_k$, where θ_k is the angular segment width of the single written contour. In Figure 4b, an HBR with a total of ten diffractive contours is analyzed. The sidelobes calculated are weaker and they appear broadened. The broadening effect arises from the variation in the magnitude of θ_k within the HBR structure. The random angular shift between the scribing patterns of successive diffractive contours has the effect of introducing random phase changes onto the fields contributed by each contour to the sidelobes. These phase changes do not affect the primary image. Owing

to the random phase shifts, the sidelobes should decrease in power relative to the primary image by a factor of approximately $1/N_c$ (based on random-walk analysis). The variation in θ_k and the random angular shifts together result in approximately one and a half orders of magnitude reduction in sidelobe power relative to the primary image (center peak) even when only 10 contours are written. In Figures 4c and 4d, the output plane power distribution for N_c=100 and N_c=1000 contours, respectively are displayed. The 1000-contour HBR has a simulated sidelobe reduction of approximately 4-orders of magnitude relative to the primary image. Simulation of the full 13305-contour fabricated HBR was not performed owing to computational limitations.

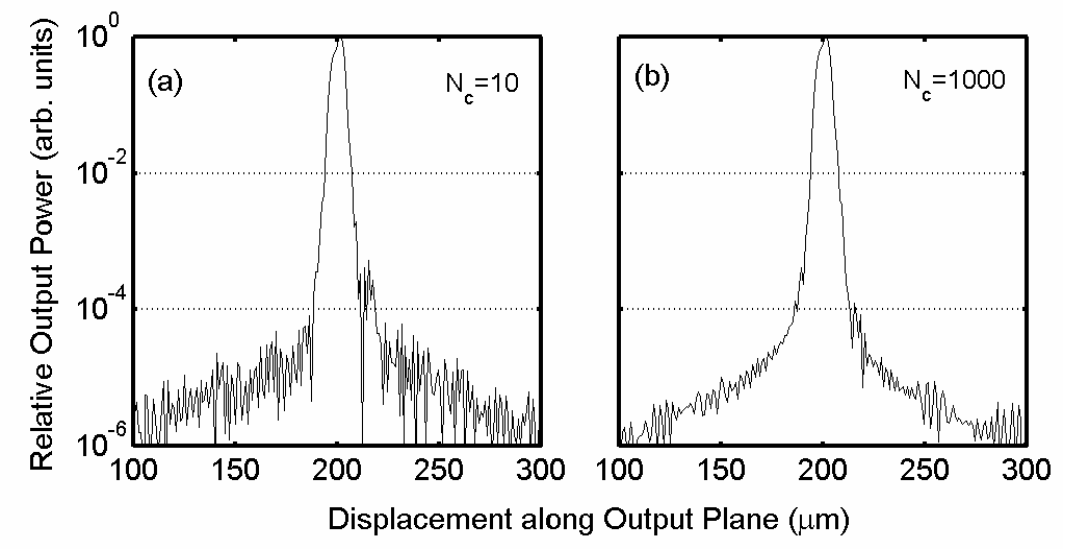

Figure 5. Simulated output power as a function of position along output plane for (a) 10 and (b) 1000 fully written continuous diffractive contours. The primary output image is located at 200 μm.

In Figure 5, we present simulations of HBRs comprised of fully written diffractive contours (no gray scale). The absence of sidelobes in Figure 5, serves to confirm the introduction of gray-scale partial scribing as the source of the sidelobes observed in Figure 4.

Measurements of power versus position along the output plane were accomplished by scanning a cleaved single-mode, SMF-28, fiber along a line parallel to the planar waveguide edge. The die and fiber were square cut and the fiber axis was oriented normal to the die edge (i. e. butt-coupled). In Figure 6a, we plot (solid line) output power versus position for a fully written first-order HBR with the input signal wavelength set to maximize HBR reflectivity. The dotted line at the bottom represents the scattered light background level as measured with the input laser tuned 20 nm above the HBR resonance wavelength. The focused HBR output is centered at 200 μm while the diffractive-contour center of curvature is located at 0 and the input signal enters at -200 μm. The measured output power profile of Figure 6a is in quite good agreement with the simulated power profile of Figure 6b considering that background is not subtracted from the solid line data of Figure 6a. The minimum insertion loss for the measurement of Figure 6a is 3.8 dB, which includes losses from fiber-to-planar-waveguide coupling. The solid line of Figure 6b represents measured output power versus output plane position produced by a first-order HBR with each diffractive contour written at the gray-scale level of 0.33. As in Figure 6a, the dotted line represents off-resonance scattered-light background. Fluctuations of background level with input-signal wavelength and detailed alignment appears to be responsible for the dips in observed output power below the off-resonance background level. The minimum insertion loss for the data of Figure 6b is 10.8 dB, again including coupling loss. In the limit of low reflectivity for both gratings, the peak reflected powers of Figure 6b and Figure 6a should be in the ratio of $(0.33)^2$:1 or -9.6 dB. The measured ratio is larger than this because the fully written first-order grating (Figure 6a) is in the regime of moderately high reflectivity. In Figure 6c, we superimpose the output power profiles of the fully (solid curve) and partially written HBRs and normalize them to the same peak value. Presented in this way, one can clearly see small sidelobes at approximately 150 μm and 250 μm on the output plane in the measured output power from the partially

written HBR (dot-dashed line). The spatial location of the observed sidelobes agrees well with the location expected on the basis of the simulation shown in Figure 4d. The side lobe magnitude observed is somewhat larger than the $\approx 10^{-5}$ expected on the basis of Figure 4 extrapolated to the case of 13305 diffractive contours. The 40 dB contrast observed between the primary output peak and the gray-scale sidelobe is, however, fully adequate for many applications. It should be noted that the simulated and fabricated partially written HBRs have not been optimized for sidelobe suppression. The angular pattern shifts and variation in θ_k may be deterministically controlled during design for more effective sidelobe suppression.

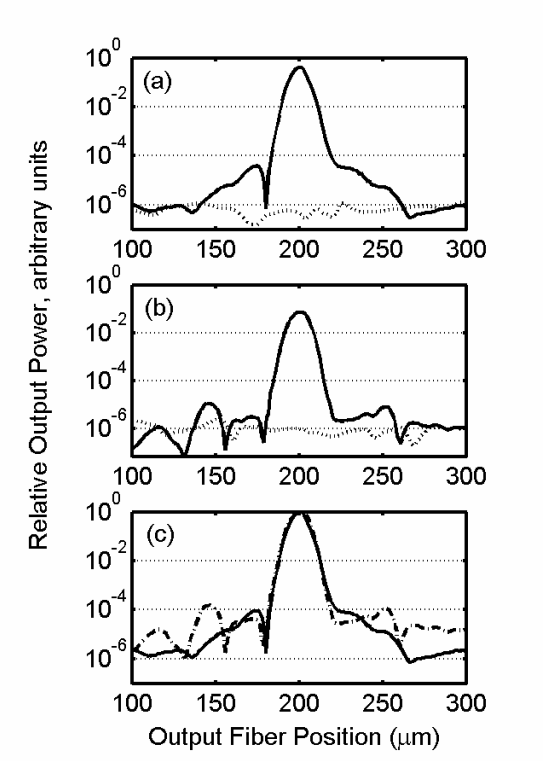

Figure 6. Measured output power as a function of position along output plane for (a) fully written first-order HBR, (b) partially written (0.33 fraction) first-order HBR, (c) superimposed fully and partially written HBR measurements. The lower dotted line in (a) and (b) represents a background light power level corresponding primarily to input signal scattered off the square-cut die boundaries.

3. CONCLUSIONS

In summary, we have studied the use of partial diffractive element scribing as a means of achieving precise reflective amplitude control in distributed 2D diffractive structures. We find that the spatial imaging and spectral properties of HBR devices are left intact through use of partial contour scribing provided that simple sidelobe suppression design features are incorporated. We find that overall reflective strength scales as expected with the fraction of diffractive contours scribed with trenches. Demonstration of these performance factors is crucial in the implementation of effective gray scale methods for general apodization of 2D spectral devices. A remaining factor to be studied is the ability to adjust separations between contours in a heavily apodized structure to compensate for small effective refractive index changes introduced in the process of changing contour fill factors. We point out that partial-fill gray scale can be implemented in slightly modified form in channel waveguide gratings. We also note that partial-fill gray scale is fully consistent with stamping-based replication of HBR and other distributed reflector devices.

REFERENCES

1. T. Erdogan, "Fiber Grating Spectra, " J. Lightwave Tech. **15**, 1277-1294 (1997).
2. J. L. Rebola and A. V. T. Cartaxo, "Performance Optimization of Gaussian Apodized Fiber Bragg Grating Filters in WDM Systems," J. Lightwave Tech. **8**, 1537-1544 (2002).
3. A. Carballar, M. A. Muriel, and J. Azana, "Fiber Grating Filter for WDM Systems: An Improved Design," Photonics Tech. Lett. **11**, 694-696 (1999).
4. T. Komukai, K. Tamura, and M. Nakazawa, "An Efficient 0.04-nm Apodized Fiber Bragg Grating and Its Application to Narrow-Band Spectral Filtering," Photonics Tech. Lett. **9**, 934-936 (1997).
5. C. Marra, A. Nirmalathas, D. Novak, C. Lim, L. Reekie, J. A. Besley, C. Weeks, and N. Baker, "Wavelength-Interleaved OADMs Incorporating Optimized Multiple Phase-Shifted FBGs for Fiber-Radio Systems," J. Lightwave Tech. **21**, 32-39 (2003).
6. K. O. Hill, B. Malo, F. Bilodeau, S. Theriault, D. C. Johnson, and J. Albert, "Variable-spectral-response optical waveguide Bragg grating filters for optical signal processing," Opt. Lett. **20**, 1438-1440 (1995).
7. A. Grunnet-Jepsen, A. E. Johnson, E. S. Maniloff, T. W. Mossberg, M. J. Munroe, and J. N. Sweetser, "Fibre Bragg grating based spectral encoder/decoder for lightwave CDMA," Electron. Lett. **35**, 1096-1097 (1999).
8. D. Wiesmann, C. David, R. Germann, D. Erni, and G. L. Bona, "Apodized Surface-Corrugated Gratings With Varying Duty Cycles," Phot. Tech. Lett. **12**, 639-641 (2000).
9. D. Wiesmann, R. Germann, G. L. Bona, C. David, D. Erni, and H. Jackel, "Add-drop filter based on apodized surface-corrugated gratings," J. Opt. Soc. Am. B **20**, 417-423 (2003).
10. Y. Shibata, T. Tamamura, S. Oku, and Y. Kondo, "Coupling Coefficient Modulation of Waveguide Grating Using Sampled Grating," Photon. Tech. Lett. **6**, 1222-1224 (1994).
11. T. W. Mossberg, "Planar holographic optical processing devices", Opt. Lett. **26**, 414 (2001).
12. C. Greiner, D. Iazikov, and T. W. Mossberg, "Lithographically scribed, focusing, planar holographic Bragg reflector with 17-GHz passband and 0.3 cm2 footprint," presented at the Optical Fiber Communication Conference, post-deadline paper PD31, Atlanta, Georgia, USA, March 23-28, 2003.
13. T. Erdogan and D. G. Hall, "Circularly Symmetric Distributed Feedback Laser: Coupled Mode Treatment of TE Vector Fields," J. Quant. Electron. **28**, 612-623 (1992).
14. R. H. Jordan and D. G. Hall, "Highly directional surface emission from concentric-circle gratings on planar optical waveguides: the field expansion method," J. Opt. Soc. Am. A **12**, 84-94 (1995).
15. R. H. Jordan, D. G. Hall, O. King, G. Wicks, and S. Rishton, "Lasing behavior of circular grating surface emitting semiconductor lasers," J. Opt. Soc. Am. B **14**, 449-453 (1997).
16. A. A. Tovar and G. H. Clark, "Concentric-circle-grating, surface-emitting laser beam propagation in complex optical systems," J. Opt. Soc. Am. A **14**, 3333-3340 (1997).
17. C. Olson and D. G. Hall, "Azimuthal Mode Discrimination in Radially Chirped Concentric-Circle-Grating Distributed Feedback Lasers," J. Quant. Electron. **36** 1016-1025 (2000).
18. S. Kristjansson, N. Eriksson, A. Larsson, R. S. Penner, and M. Fallahi, "Observation of stable cylindrical modes in electrically pumped circular grating-coupled surface-emitting lasers," Appl. Opt. **39**, 1946-1953 (2000).